# Direct Measurement of the Spatial Damping of Capillary Waves at Liquid–Vapor Interfaces

**Ka Yee Lee,† Tom Chou, Doo Soo Chung,‡ and Eric Mazur***

*Department of Physics and Division of Applied Sciences, Harvard University, Cambridge, Massachusetts 02138*

*Received: June 28, 1993; In Final Form: August 31, 1993**

We measured the spatial damping of low-frequency surface waves at air–water interfaces using a novel heterodyne light-scattering technique. For pure water the measured damping agrees well with linear hydrodynamic theory. For interfaces covered with a monolayer of pentadecanoic acid, we find a 5-fold increase in damping at a surface concentration of 2.2 molecules $nm^{-2}$, near the high-density end of the gas/liquid-expanded coexistence region. The behavior of the damping as a function of surface concentration cannot be explained by existing theories.

The study of interfaces has attracted the attention of scientists throughout history. It has been known for a long time, for example, that a single surfactant monolayer at a liquid–vapor interface can lead to a dramatic attenuation of wave motion.[1,2] Recently, because of the many technological applications of surfactants and because of the biological importance of monolayer films, the properties of these quasi-two-dimensional systems have been the subject of renewed interest. In spite of much research, however, there still is a lack of experimental data on surface viscoelastic properties. Yet the damping of surface waves has been attributed to these viscoelastic constants.[3] Measurements of surface wave damping can therefore furnish information on surface viscoelastic properties.

A number of groups have used inelastic light scattering to study the damping of thermally excited capillary waves[4,5] caused by spontaneous fluctuations. In principle, the temporal damping coefficient can be obtained from the width of the inelastic peaks in the spectrum of the scattered light.[6] In practice, however, these peaks are instrumentally broadened. There is no direct method to determine the instrumental broadening, which frequently dominates the width, especially in the low-frequency regime. Other groups have studied capillary wave damping by looking at the deflection of a laser beam[7] by induced surface waves.[8] This technique works only for low-frequency surface waves, when the laser spot size is smaller than the surface wavelength. The results presented here were obtained using a novel differential light-scattering technique that is free of the difficulties mentioned above. We present data on capillay wave damping for pure water and pentadecanoic acid (PDA).

Interfacial waves of small amplitude caused a normal displacement of the interface, $\zeta = \zeta_0 \exp[i(kx - \omega t)]$, with $\zeta_0$ the amplitude of the wave, $k$ the wavevector, $\omega$ the frequency, and $x$ the direction of propagation along the surface. From the linearized Navier–Stokes equation one obtains the following dispersion relation for waves on a liquid–vapor interface:[9]

$$[\sigma k^3 + \rho g k + i\eta\omega_0 k(k+m)\rho\omega_0^2][\epsilon k^2 + i\eta\omega_0(k+m)] + \omega_0^2\eta^2 k(k-m)^2 = 0 \quad (1)$$

with

$$m = k\sqrt{1 + i\omega_0\rho/\eta k^2}$$

and where $\eta$ is the dynamic viscosity, $\rho$ the density of the liquid, $g$ the gravitational acceleration, and $\sigma$ the equilibrium surface tension. In the absence of surface viscosity, $\epsilon$ is the complex surface dilation modulus.

For a pure interface ($\epsilon = 0$) in the low-viscosity limit, the frequency of a wave with real wavevector $k$, $\omega = \omega_0 - i\beta$, has a small imaginary component, $\beta = 2k_0^2\eta/\rho$, leading to temporal damping of the wave. This coefficient $\beta$ can be obtained from the widths of the inelastic peaks in the spectrum of the light scattered from thermal capillary waves but requires deconvolution of instrumental line broadening.[4,5] Alternatively, the wavevector for a wave of fixed real frequency $\omega_0$, has a small imaginary part contributing to spatial damping. Substituting $k = k_0 + i\alpha$ ($\alpha \ll k_0$) into eq 1 with $\epsilon = 0$, keeping only first-order terms in $\nu$ and $\alpha$ and neglecting the gravity term, we obtain

$$\alpha = 4\eta\omega_0/3\sigma \quad (2)$$

The spatial damping coefficient $\alpha$ is therefore related to $\beta$ by $\beta = \alpha\, \partial\omega/\partial k$. In the experiment described below the spatial damping coefficient $\alpha$ is determined by measuring the exponential decay $e^{-\alpha x}$ of the amplitude of an induced surface wave.

In our experiment capillary waves of frequency $f_0 \equiv \omega_0/(2\pi)$ in the 0.5–2 kHz range are generated by applying a sinusoidal voltage ($\sim$ 100 V) of frequency $f_0/2$ to a metal blade placed about 1 mm from the interface.[7] For pure water, where eq 1 reduces to $\omega^2 = (\sigma/\rho)k^3 + gk$, these frequencies yield wavelengths of 0.5–1.2 mm. To probe the wave amplitude as a function of distance $x$, we use a heterodyne light-scatering technique described previously.[10] Since translating the probe spot is not practical, one must translate the blade to vary $x$. To compensate for any variation in the distance between the blade tip and the surface during translation, we use a differential technique and measure the ratio between wave amplitudes on both sides of the blade.

A schematic diagram of the experimental setup is shown in Figure 1. A 10-mW He–Ne laser beam is split into a main beam (M) and a much weaker (5%) local oscillator (LO). The frequency of the two beams is shifted using a pair of acoustooptic modulators, giving the beams a frequency difference $\Delta f = 5.1$ kHz.[10] The M and LO beams are focused onto a single 2-mm-diameter spot on the surface at an incidence angle of about 60°. The angle between the two beams is adjusted so as to make the difference of the incident light wavevectors match the induced surface wavevector.

An identical pair of M and LO beams is focused onto a second probe spot on the other side of the blade at a fixed distance $d$ = 40 mm from the first. Since the induced waves travel in opposite directions at the two probe spots, the detected signals are at frequencies $\Delta f - f_0$ and $\Delta f + f_0$, respectively (see Figure 1). The two scattered light beams are combined and detected with a single photomultiplier tube. The photomultiplier signal is digitized at a 20-kHz rate and then Fourier-transformed to obtain the power spectrum of the scattered light.[10]

A typical spectrum is shown in Figure 2. It consists of an intense central peak at the carrier frequency $\Delta f$, and satellite peaks centered at $\Delta f \pm f_0$. The two sharp peaks result from the

† Current address: Department of Chemistry, Stanford University, Stanford, CA 94305-5080.
‡ Current address: Department of Physics, Massachusetts Institute of Technology, Cambridge, MA 02139.
* Abstract published in *Advance ACS Abstracts*, October 15, 1993.

0022-3654/93/2097-12876$04.00/0 

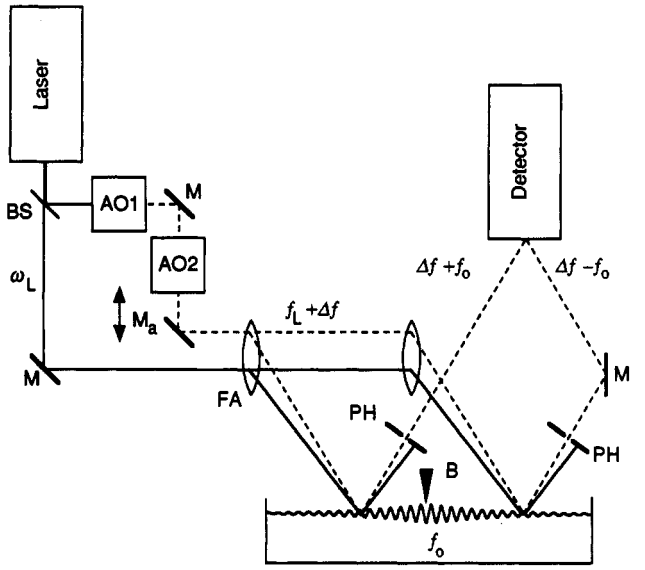


**Figure 1.** Schematic diagram of apparatus. AO = acoustooptic modulator; B = electrocapillarity blade; BS = beam splitter; FA = focusing assembly; M = mirror; PH = pinhole. The dashed line is the local oscillator; the solid line is the main laser beam.

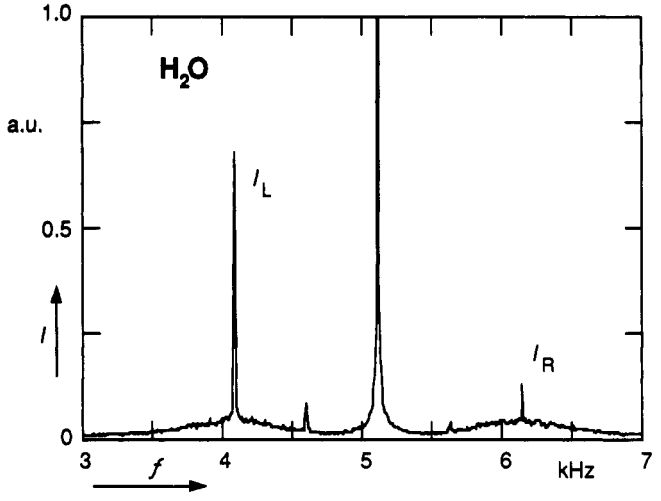


**Figure 2.** Frequency spectrum for pure water at 23.5 °C. The amplitude ratio $I_L/I_R$ of the sharp peaks due to the induced surface wave is proportional to the surface wave amplitude ratio $A_L/A_R$. The small peaks at $\Delta f \pm f_0/2$ ($\Delta f$ = 5.1 kHz; $f_0$ = 1.2 kHz) are due to the fundamental frequency $f_0/2$ applied to the blade for generating capillary waves at frequency $f_0$.

induced surface waves traveling in opposite directions, while the two broad peaks (at the base of the sharp ones) are due to thermally excited capillary waves. Since height of the sharp peaks is directly proportional to the amplitude of induced surface waves, the ratio of the peak heights equals the amplitude ratio of the induced wave amplitudes at the two probe spots. For the geometry shown in Figure 1, the wave amplitudes at the probe spots are $A_L = c_L\zeta_0 \exp(-\alpha x)$ and $A_R = c_R\zeta_0 \exp[-\alpha(d-x)]$ on the left and the right of the blade, respectively; $\zeta_0$ is the wave amplitude at the source and the $c$'s are instrumental constants. The ratio $A_L/A_R = c_L/c_R \exp(\alpha d) \exp(-2\alpha x) = c \exp(-2\alpha x)$ is now *independent* of the source wave amplitude $\zeta_0$. We verified experimentally that the ratio $A_L/A_R$ was independent of the wave amplitude over a range of amplitudes from 2 to 300 nm.

The sample surface is contained in a temperature-controlled Langmuir trough (305 × 76 × 5 mm³) of Teflon-coated stainless-steel. To prevent contamination of the surface, the trough is cleaned and placed inside a sealed compartment filled with ultrapure nitrogen with less than 0.5 ppm total hydrocarbon content. After filling the trough with distilled and deionized

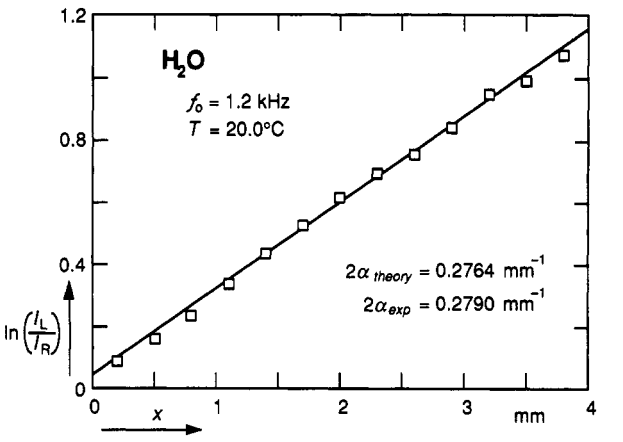


**Figure 3.** Surface wave amplitude ratio as a function of distance showing spatial decay of surface wave for pure water at 23.5 °C. The solid line shows the expected behavior using literature values for the surface tension and shear viscosity of water.

water from a Millipore Milli-Q UV system, the liquid surface is aspirated to remove residual contaminants. The surface tension is monitored with a surface balance. The entire setup is put on an actively stabilized platform, which in turn is positioned on a pneumatically vibration-isolated table.

Figure 3 shows the exponential decay of a 1.2-kHz surface wave on pure water at 23.5 °C. The horizontal distance between each of the points corresponds to a blade transition step. The vertical axis is the ratio of peak heights $I_L/I_R \propto A_L/A_R$ taken directly from spectra such as the one shown in Figure 2. The slope yields a spatial damping coefficient $\alpha = 0.1395$ mm$^{-1}$. Using literature data[11] for $\eta$ and $\sigma$ in eq 2 yields $\alpha = 0.1382$ mm$^{-1}$, in excellent agreement with our measured value. Results for $\alpha$ for waves of frequency 0.5–2.0 kHz at 23.5 °C agree also with the linear frequency dependence expressed in eq 2. This agreement between measured and calculated damping coefficients was further verified to hold over a temperature range frm 14 to 41 °C.

To study the influence of a monolayer of PDA on the surface-wave damping, we measured the damping of 0.8-, 1.0-, and 1.2-kHz surface waves at different surface concentrations of PDA (Aldrich, 99.9%). The surface concentration is varied by spreading controlled amounts of a solution of PDA in chloroform on the water surface. To prevent the PDA from dissociating and dissolving into the bulk, the pH of the water was adjusted to about 2 by adding hydrochloric acid. After each addition of PDA the chloroform was let to evaporate for at least 20 min and the chamber flushed a few times with ultrapure nitrogen. Then, the system was allowed to mechanically and thermally equilibrate for at least 3 h before taking optical and surface pressure measurements. It takes about 4 s to obtain a single spectrum at a fixed blade position (as in Figure 2); The damping coefficient at a particular surfactant concentration is obtained from a series of measurements at different blade positions taken over 15 min (see in Figure 3). After each change in concentration, the system is again allowed at least 3 h to reach a steady surface tension.

Figure 4 shows the measured spatial damping coefficient $\alpha$ and surface pressure $\Pi$ (the deviation of the surface tension from its value for a pure interface) as a function of surface concentration $\Gamma$ at 20.1 °C and 1.2 kHz. Measurements carried out at 0.8 and 1.0 kHz show a similar behavior. At low surface concentration the damping coefficient is equal to that of pure water. At $\Gamma \approx$ 1 molecule nm$^{-2}$, $\alpha$ starts to increase with increasing surface concentration. The accompanying surface pressure data, which are in excellent agreement with previously published results,[12] indicate that the monolayer is in the liquid-expanded (LE)/gaseous (G) coexistence region at this concentration. At about 2.2 molecules nm$^{-2}$ the spatial damping reaches a maximum of approximately 5 times the value at $\Gamma = 0$. At the same time, the

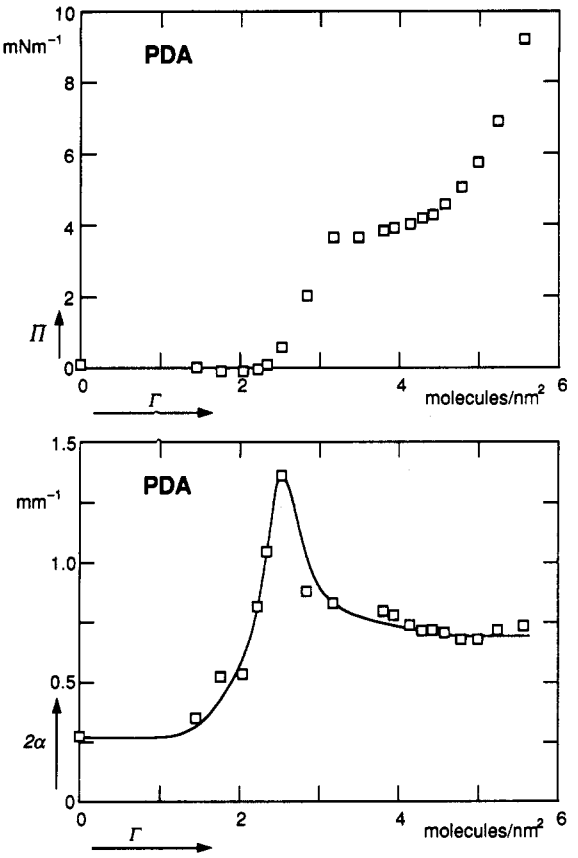


**Figure 4.** Surface pressure (top) and spatial damping (bottom) as a function of surface concentration of PDA for water at 20.1 °C.

surface pressure starts to increase sharply, marking the end of the G/LE coexistence region and the beginning of the LE phase. As the surface concentration is further increased, the damping coefficient decreases and finally levels out. Measurements of the temporal damping coefficient also show a maximum near the high-concentration end of the liquid-expanded/gaseous coexistence region.[13]

A maximum in the spatial damping coefficient occurring at some intermediate value of the surface bulk modulus has been predicted as early as 1951 by Dorrestein[3] and others.[9] Contrary to our data, these theories predict a damping value equal to that of a clean interface whenever the isothermal bulk moduli vanish, *i.e.*, in coexistence regions. Since our experiments are done at kilohertz frequencies the bulk moduli may not be zero. In this case the damping coefficient would depend on the wave amplitude. Experiments to investigate the dependence of the damping coefficient on the wave amplitude are currently in progess.

A factor not considered by the hydrodynamical theories is the effect of heterogeneity when the surface film undergoes a first-order transition. Indeed, mesoscopic domains ranging from microns to millimeters in size have been observed using fluorescence[14,15] and Brewster-angle microscopy.[16,17] Heterogeneities may affect wave propagation by changing the effective surface properties for domains much smaller than the wavelength $\lambda \approx 0.5$–$1.2$ mm of the wave or by scattering the surface waves when domain sizes are of order $\lambda$. While the importance of these effects is not known, our measurements still produce an effective damping constant reflecting the inhomogeneous and probably random distribution of surfactant domains. This is so because the distance between the blade and detection spot (about 20 mm) is much larger than the size of the domains. Understanding the effects of heterogeneities on the damping of surface waves will require further theoretical as well as experimental research.

In summary, we have measured the spatial damping coefficients of low-frequency capillary waves, using heterodyne light scattering. The technique has a wide dynamic range and requires no deconvolution or calibration. The coefficients obtained for a pure air–water interface at different frequencies agree with what linear hydrodynamic theory predicts. For a surface covered with a PDA monolayer, however, the behavior of the spatial damping coefficient is not adequately described by existing theories. In particular, we observe a maximum in the damping at the junction between the LE/G coexistence region and the LE phase. These measurements also suggest that the damping coefficient could be a useful tool for probing phases of monolayers. We are currently investigating the temperature and wave-amplitude dependence of the damping coefficient. These results will be published in a forthcoming paper.

**Acknowledgment.** We gratefully acknowledge many useful discussions with Professor David Nelson. This work was supported by National Science Foundation Contract DMR 88-58075. T.C. acknowledges the support of a National Science Foundation graduate fellowship.

## References and Notes

(1) Plinius, *Historia Naturalis*; 1st century A.D.
(2) Franklin, B. *R. Soc. Faraday Trans.* **1774**, *64*, 445.
(3) Dorrestein, R. *Proc. K. Ned. Akad. Wet., Ser. B: Paleontol., Geol., Phys. Chem.* **1951**, *54*, 260.
(4) Thominet, V.; Stenot, C.; Langevin, D. *J. Colloid Interface Sci.* **1988**, *126*, 54.
(5) Earnshaw, J. C.; McGivern, R. C.; Winch, P. J. *J. Phys. (Paris)* **1988**, *49*, 1271.
(6) Langevin, D. *J. Chem. Soc.* **1974**, *70*, 95.
(7) Sohl, C. H.; Miyano, K.; Ketterson, J. B. *Rev. Sci. Instrum.* **1978**, *49*, 1464.
(8) Stenvot, C.; Langevin, D. *Langmuir* **1988**, *4*, 1179–1183.
(9) Lucassen-Reynders, E. H.; Lucassen, J. *Adv. Colloid Interface Sci.* **1969**, *2*, 347.
(10) Mazur, E.; Chung, D. S. *Physica* **1987**, *147A*, 387.
(11) *CRC Handbook of Chemistry and Physics*; Weast, R. C., Ed.; CRC Press, Inc.: Boca Raton, FL, 1985–1986.
(12) Pallas, N. R.; Pethica, B. A. *J. Chem. Soc., Faraday Trans 1* **1987**, *83*, 585–590.
(13) Chen, Y. L.; Sano, M.; Kaawaguchi, M.; Yu, H.; Zografi, G. *Langmuir* **1986**, *2*, 349.
(14) McConnell, H. M. *Annu. Rev. Phys. Chem.* **1991**, *42*, 171–195.
(15) Knobler, C. M. *Adv. Chem. Phy.* **1990**, *77*, 397.
(16) Honig, D.; Mobius, D. *J. Phys. Chem.* **1991**, *95*, 4590–4592.
(17) Henon, S.; Meunier, J. *Rev. Sci. Instrum.* **1990**, *62*, 936–939.